

## Resonant Relaxation in Stellar Systems

Kevin P. Rauch and Scott Tremaine  
Canadian Institute for Theoretical Astrophysics,  
University of Toronto,  
60 St. George St., Toronto M5S 3H8, Canada

### ABSTRACT

We demonstrate the existence of an enhanced rate of angular momentum relaxation in nearly Keplerian star clusters, such as those found in the centers of galactic nuclei containing massive black holes. The enhanced relaxation arises because the radial and azimuthal orbital frequencies in a Keplerian potential are equal, and hence may be termed *resonant relaxation*. We explore the dynamics of resonant relaxation using both numerical simulations and order-of-magnitude analytic calculations. We find that the resonant angular momentum relaxation time is shorter than the non-resonant relaxation time by of order  $M_*/M$ , where  $M_*$  is the mass in stars and  $M$  is the mass of the central object. Resonance does not enhance the energy relaxation rate. We examine the effect of resonant relaxation on the rate of tidal disruption of stars by the central mass; we find that the flux of stars into the loss cone is enhanced when the loss cone is empty, but that the disruption rate averaged over the entire cluster is not strongly affected. We show that relativistic precession can disable resonant relaxation near the main-sequence loss cone for black hole masses comparable to those in galactic nuclei. Resonant dynamical friction leads to growth or decay of the eccentricity of the orbit of a massive body, depending on whether the distribution function of the stars is predominantly radial or tangential. The accelerated relaxation implies that there are regions in nuclear star clusters that are relaxed in angular momentum but not in energy; unfortunately, these regions are not well-resolved in nearby galaxies by the Hubble Space Telescope.

*Subject headings:* black hole physics — galaxies: active — galaxies: kinematics and dynamics — galaxies: nuclei — stellar dynamics

The dynamical evolution of galactic and active galactic nuclei (AGNs) is determined by numerous physical processes, including two-body relaxation, stellar collisions/mergers, tidal disruption, binary formation, stellar evolution, and disk hydrodynamics (e.g., Spitzer & Stone 1967; Norman & Scoville 1988; Quinlan & Shapiro 1990; Murphy et al. 1991). In most cases, however—and in contrast to systems such as globular clusters—the two-body relaxation times are so long that relaxation has had little observable effect on the nucleus so far. The slow relaxation rates in galactic nuclei are responsible, for example, for the general failure of stellar tidal disruption by relaxation into the loss cone (Frank & Rees 1976; Lightman & Shapiro 1977) as a viable AGN fueling mechanism (Hills 1975; Frank 1978; McMillan et al. 1981), and for the absence of core collapse or mass segregation at observable resolutions in all but a few nearby galaxies (e.g., M33; Kormendy & McClure 1993).

Normally the gravitational potential in a galaxy is determined by the stars and distributed dark matter. However, in galactic nuclei possessing massive black holes, the potential in the inner nucleus is dominated by the black hole and hence nearly Keplerian, so that eccentric orbits maintain their spatial orientation for many orbital periods. The aim of this paper is to demonstrate that in Keplerian and other such “resonant” potentials the rate of relaxation of angular momentum can be greatly enhanced, so that relaxation can be important even if the energy relaxation timescale is longer than a Hubble time. We examine the dynamics of this “resonant relaxation” through approximate analytic arguments and  $N$ -body simulations, and discuss its influence on galactic nuclei.

## 1. The Process of Resonant Relaxation

### 1.1. Introduction

The force field  $\mathbf{F}(\mathbf{r}, t)$  in an equilibrium  $N$ -body stellar system can be divided into a mean force  $\overline{\mathbf{F}}(\mathbf{r}) \equiv \langle \mathbf{F}(\mathbf{r}, t) \rangle$  and a fluctuating force  $\mathbf{f}(\mathbf{r}, t) \equiv \mathbf{F}(\mathbf{r}, t) - \overline{\mathbf{F}}(\mathbf{r})$ , where  $\langle \cdot \rangle$  denotes time average. If  $N \gg 1$  the fluctuating force is a Gaussian random field, and hence is completely described by the correlation function  $C_{ij}(\mathbf{r}_1, \mathbf{r}_2, \tau) \equiv \langle f_i(\mathbf{r}_1, t), f_j(\mathbf{r}_2, t + \tau) \rangle$ . This fluctuating force induces diffusion or relaxation of the deterministic orbits that stars would follow if only the mean force field  $\overline{\mathbf{F}}$  were present. The relaxation time,  $t_{\text{rel}}$ , is crudely defined so that the diffusion of integrals of motion such as energy  $E$  and angular momentum  $L$  (per unit mass) is given by  $\Delta E \sim E (t/t_{\text{rel}})^{1/2}$  and  $\Delta L \sim L (t/t_{\text{rel}})^{1/2}$ .

The usual estimate of the relaxation time (Jeans 1913, 1916; Chandrasekhar 1942; Binney & Tremaine 1987) is based on an infinite homogeneous stellar system in which stars

travel on straight-line orbits. This assumption is plausible because each octave in spatial scale between the system size  $R$  and the much smaller scale  $r_{\min} \sim R/N$  (the scale on which close encounters produce  $\sim 90^\circ$  deflections) contributes equally to the relaxation rate, and for most of these octaves the approximations of homogeneity and straight-line orbits are legitimate (summing the contributions from different scales gives rise to the well-known Coulomb logarithm  $\ln \Lambda \simeq \ln(R/r_{\min}) \simeq \ln(N)$  which appears in formulae for the relaxation rate). One consequence of the assumption of straight-line orbits is that the correlation function  $C_{ij}(\mathbf{r}_1, \mathbf{r}_2, \tau)$  decays rapidly to zero when  $\tau$  exceeds  $|\mathbf{r}_1 - \mathbf{r}_2|/V$ , where  $V$  is a typical velocity (for infinite homogeneous systems  $C_{ij} \rightarrow 1/\tau$  as  $\tau \rightarrow \infty$  [e.g. Cohen 1975]). Our focus here is on stellar systems in which the correlation function remains non-zero for much larger times, a condition that occurs if most of the stars are near resonance.

If motion in the mean force field  $\overline{\mathbf{F}}(\mathbf{r})$  is regular, then stellar orbits are quasiperiodic with three characteristic frequencies  $\Omega_i$ . The orbits are resonant if there are linear combinations of the form  $\sum_{i=1}^3 k_i \Omega_i = 0$  where the  $k_i$  are small integers. The simplest important examples are (i) spherical potentials, in which one frequency is zero because all orbits remain in a fixed plane; (ii) Kepler potentials, in which one additional frequency is zero because the apsis does not precess; and (iii) the harmonic oscillator potential, in which the radial frequency is twice the azimuthal frequency, so that the orbit shape is a centered ellipse.

The possibility of enhanced relaxation in potentials that support many near-resonant orbits was discussed by J. Ostriker two decades ago, in lectures for a graduate course in stellar dynamics attended by one of us (Ostriker 1973).

## 1.2. Non-resonant Relaxation

We begin by examining relaxation in a near-Kepler potential. Consider a spherical volume of radius  $R$  centered on a point mass  $M$  and containing  $N \gg 1$  identical stars of mass  $m$ , where  $M_\star \equiv Nm \ll M$ . We assume that the stellar orbits have random orientations and moderate eccentricities, and that the density of stars is approximately uniform within  $R$ . The typical stellar velocity is  $V \sim (GM/R)^{1/2}$  and the characteristic orbital period is  $t_{\text{orb}} \sim R/V$ . Since  $M_\star \ll M$ , each orbit is approximately a Kepler ellipse, which precesses slowly on a timescale  $t_{\text{prec}}$ . If the precession is dominated by the mean field from the other stars (rather than, say, relativistic effects or an external tidal field), then

$$t_{\text{prec}} \sim \frac{M}{M_\star} t_{\text{orb}}, \quad (1)$$

which is much longer than  $t_{\text{orb}}$ .

The usual (non-resonant) relaxation rate can be estimated by the following argument. Consider a volume of radius  $r < R$ , which typically contains  $n \sim N (r/R)^3$  stars. The instantaneous number of stars in this volume fluctuates by an amount  $n^{1/2}$ ; thus the fluctuating force on the length scale  $r$  is  $f \sim Gmn^{1/2}/r^2$ . The force fluctuates on a timescale  $t_f \sim r/V$ , and the typical impulse that a star receives during this timescale is  $\delta v \sim ft_f \sim Gmn^{1/2}/(rV)$ . Since impulses in successive intervals of length  $t_f$  are uncorrelated, the total impulse after time  $t$  is described by a random walk,

$$(\Delta v)^2 \sim (\delta v)^2 \frac{t}{t_f} \sim \frac{G^2 m^2 n}{r^3 V} t \sim \frac{G^2 m^2 N}{R^3 V} t \sim V^2 \frac{m^2 N}{M^2} \frac{t}{t_{\text{orb}}}. \quad (2)$$

Note that  $\Delta v$  is independent of the scale  $r$ , which confirms that each octave in scale contributes equally to the relaxation rate; thus the total diffusion rate must be multiplied by a factor  $\ln \Lambda$  which represents the number of octaves that contribute to the relaxation. We may define the non-resonant relaxation time by  $(\Delta v/V)^2 = (t/t_{\text{rel}}^{\text{nr}})$ , so that

$$t_{\text{rel}}^{\text{nr}} \sim \frac{M^2}{m^2 N \ln \Lambda} t_{\text{orb}}. \quad (3)$$

The fluctuating force changes both energy and angular momentum, at rates given by

$$\begin{aligned} (\Delta E/E)_{\text{nr}} &\sim (t/t_{\text{rel}}^{\text{nr}})^{1/2} \sim \alpha \frac{mN^{1/2}}{M} (t/t_{\text{orb}})^{1/2}, \\ (\Delta L/L_{\text{max}})_{\text{nr}} &\sim (t/t_{\text{rel}}^{\text{nr}})^{1/2} \sim \eta_s \frac{mN^{1/2}}{M} (t/t_{\text{orb}})^{1/2}, \end{aligned} \quad (4)$$

where  $E \sim V^2 \sim GM/R$ ,  $L_{\text{max}}^2 \sim V^2 R^2 \sim GMR$ , and  $\alpha$  and  $\eta_s$  are dimensionless constants that equal the square root of the Coulomb logarithm to within a factor of order unity.

### 1.3. Resonant Relaxation in Near-Kepler Potentials

To estimate the resonant relaxation rate, we imagine averaging the stellar density over an intermediate timescale that is  $\gg t_{\text{orb}}$  but  $\ll t_{\text{prec}}$ . On this timescale each star can be represented by a fixed wire whose mass is the stellar mass, whose shape is a Kepler ellipse, and whose linear density is inversely proportional to the local speed in the elliptical orbit.

The gravitational potential from these wires is stationary and hence does not lead to energy relaxation; thus

$$(\Delta E/E)_{\text{res}} = 0. \quad (5)$$

However, the wires exert mutual torques which induce angular momentum relaxation. The typical specific torque on a wire is  $T \sim N^{1/2} Gm/R$ , and fluctuates on a timescale  $\sim t_{\text{prec}}$  as

the wires precess in different directions. Thus the characteristic change in specific angular momentum  $\Delta L \sim Tt$  over a timescale  $t < t_{\text{prec}}$  is given by

$$(\Delta L/L_{\text{max}})_{\text{res}} \sim \beta_s \frac{mN^{1/2}}{M} (t/t_{\text{orb}}), \quad t \ll t_{\text{prec}}, \quad (6)$$

where  $\beta_s$  is a dimensionless constant of order unity.

Over timescales  $t \gg t_{\text{prec}}$ , the change in angular momentum is described by a random walk with increments  $\Delta L/L_{\text{max}} \sim \beta_s (mN^{1/2}/M) (t_{\text{prec}}/t_{\text{orb}})$  over a characteristic time  $t_{\text{prec}}$ ; thus,

$$(\Delta L/L_{\text{max}})_{\text{res}} \sim \beta_s \frac{mN^{1/2}}{M} \left( \frac{t_{\text{prec}} t}{t_{\text{orb}}^2} \right)^{1/2}, \quad t \gg t_{\text{prec}}; \quad (7)$$

if the precession is determined by the mean field of the other stars then equation (1) implies that

$$(\Delta L/L_{\text{max}})_{\text{res}} \sim \beta_s \left( \frac{m}{M} \right)^{1/2} (t/t_{\text{orb}})^{1/2}, \quad t \gg t_{\text{prec}}. \quad (8)$$

In this case the angular momentum relaxation time, defined by  $(\Delta L/L_{\text{max}})_{\text{res}} \sim (t/t_{\text{rel}}^{\text{res}})^{1/2}$ , is given by

$$t_{\text{rel}}^{\text{res}} \sim \frac{M}{m} t_{\text{orb}}, \quad (9)$$

which, remarkably, is independent of the number of stars  $N$ . The resonant relaxation time is shorter than the non-resonant relaxation time (eq. [3]) by a factor  $(mN/M) \ln \Lambda$ . If there is a range of stellar masses, the factor  $m$  in equation (9) should be replaced by  $\int m^2 dN(m) / \int m dN(m)$ .

There is no analog to the Coulomb logarithm in resonant relaxation, since the relaxation is dominated by large-scale fluctuations. The absence of the Coulomb logarithm implies that the resonant diffusion rate depends on the overall structure of the stellar system and cannot be computed using the assumption of local homogeneity, as is done for the non-resonant relaxation rate.

On timescales longer than the resonant relaxation time but shorter than the non-resonant relaxation time, a stellar system in a Kepler potential should be in the maximum-entropy state consistent with its original total angular momentum  $\mathbf{L}_{\text{tot}}$  and energy distribution  $N(E)$  (the number of stars with energy  $< E$ , which is invariant on this timescale since there is no resonant energy relaxation). This state is described by the phase-space distribution function

$$f(\mathbf{r}, \mathbf{v}) = w(E) \exp(-\mathbf{b} \cdot \mathbf{L}), \quad (10)$$

where  $E = \frac{1}{2}v^2 - GM/r$ ,  $\mathbf{L} = \mathbf{r} \times \mathbf{v}$ , and  $\mathbf{b}$  and  $w(E)$  are determined implicitly by the constraints

$$\begin{aligned}\mathbf{L}_{\text{tot}} &= \int f(\mathbf{r}, \mathbf{v}) \mathbf{L} \, d\mathbf{r} \, d\mathbf{v}, \\ \frac{dN(E)}{dE} &= \int f(\mathbf{r}_1, \mathbf{v}_1) \delta(E - E_1) \, d\mathbf{r}_1 \, d\mathbf{v}_1.\end{aligned}\tag{11}$$

If  $\mathbf{L}_{\text{tot}} = 0$  then  $\mathbf{b} = 0$  and the distribution function is a function of energy alone (i.e., the cluster is isotropic). If there is a range of masses then (10) is replaced by

$$f(\mathbf{r}, \mathbf{v}, m) = w(E, m) \exp(-m \mathbf{b} \cdot \mathbf{L}).\tag{12}$$

#### 1.4. Resonant Relaxation in Near-spherical Potentials

A more limited form of resonant relaxation is present in *any* spherical potential. Consider a generic spherical potential and average the stellar density over a timescale  $\gg t_{\text{orb}}$ . On this timescale each star is smeared into an axisymmetric annulus whose inner and outer radii are the pericenter and apocenter distances. The gravitational potential from these annuli is stationary and hence does not lead to energy relaxation; thus, as in equation (5),

$$(\Delta E/E)_{\text{res}} = 0.\tag{13}$$

The annuli exert mutual torques which induce angular momentum relaxation; however, in contrast to the Kepler case the torques are perpendicular to the orbit normals (because the averaged orbits are axisymmetric annuli rather than eccentric wires). Thus the vector torque  $\mathbf{T}_{ij}$  between two annuli with vector angular momenta  $\mathbf{L}_i$  and  $\mathbf{L}_j$  satisfies  $\mathbf{T}_{ij} \cdot \mathbf{L}_i = \mathbf{T}_{ij} \cdot \mathbf{L}_j = 0$ ; in other words the torques change the directions of the angular momentum vectors but not their magnitudes. Thus, in contrast to equation (6), there is no resonant relaxation of the scalar angular momentum,

$$(\Delta L/L_{\text{max}})_{\text{res}} = (\Delta |\mathbf{L}|/L_{\text{max}})_{\text{res}} = 0,\tag{14}$$

but there *is* resonant relaxation of the *vector* angular momentum. The resonant relaxation rate may be estimated by analogy with equation (6). The typical specific torque on an annulus is  $T \sim N^{1/2} Gm/R$ , and fluctuates on a timescale  $\sim t_{\text{prec}}^L$ . Here  $t_{\text{prec}}^L$  is the precession time for the angular momentum vector (*not* the apsis, as in §§ 1.2 and 1.3), and is determined by the stochastic component of the potential,  $t_{\text{prec}}^L \sim N^{1/2} t_{\text{orb}}/\mu$ .

The characteristic change in vector angular momentum over a timescale  $t < t_{\text{prec}}^L$  is given by  $|\Delta \mathbf{L}| \sim Tt$ . Since we are considering general near-spherical potentials, we no

longer require that the potential is dominated by a black hole,  $M_\star \ll M$ ; thus the maximum angular momentum is given by  $L_{\max}^2 \sim V^2 R^2 \sim G(M + M_\star)R$  and we have

$$(|\Delta \mathbf{L}|/L_{\max})_{\text{res}} \sim \mu \frac{\beta_v}{N^{1/2}} (t/t_{\text{orb}}), \quad t \ll t_{\text{prec}}^L, \quad (15)$$

where  $\beta_v$  is a dimensionless constant of order unity, and

$$\mu = \frac{M_\star}{M_\star + M} \quad (16)$$

( $\sim 1$  if the potential is dominated by the stars themselves).

Over timescales  $t \gg t_{\text{prec}}^L$ , the change in angular momentum is described by a random walk. The increments  $\Delta \mathbf{L}$  of the random walk are determined by evaluating (15) at  $t \sim t_{\text{prec}}^L$ , which yields  $|\Delta \mathbf{L}|/L_{\max} \sim 1$ . In other words the angular momentum vectors drift over the whole velocity sphere on a timescale of order  $t_{\text{prec}}^L$ , implying  $t_{\text{rel}}^{\text{res}} \sim t_{\text{prec}}^L \sim N^{1/2} t_{\text{orb}}/\mu$ , which is shorter than the non-resonant relaxation time  $t_{\text{rel}}^{\text{nr}}$  (eq. [3]) by a factor  $(\mu/N^{1/2}) \ln \Lambda$ .

A closely related form of resonant relaxation is present in general axisymmetric potentials that are nearly spherical. Once again there is no resonant relaxation of the scalar angular momentum, but there is resonant relaxation of the vector angular momentum. In this case only the  $z$ -component of the vector angular momentum is conserved by motion in the mean potential, so we focus on this component. By analogy with equation (15) we have

$$(|\Delta L_z|/L_{\max})_{\text{res}} \sim \mu \frac{\beta_z}{N^{1/2}} (t/t_{\text{orb}}), \quad t \ll t_{\text{prec}}^L, \quad (17)$$

where in this case  $t_{\text{prec}}^L$ , the precession time for the angular momentum vector, is determined by the non-spherical component of the mean potential. Over timescales  $\gg t_{\text{prec}}^L$ , the change in  $L_z$  is described by a random walk with increments  $|\Delta L_z|/L_{\max} \sim (\mu\beta_z/N^{1/2})(t_{\text{prec}}^L/t_{\text{orb}})$  over a characteristic time  $t_{\text{prec}}^L$ ; thus,

$$(|\Delta L_z|/L_{\max})_{\text{res}} \sim \mu \frac{\beta_z}{N^{1/2}} \left( \frac{t_{\text{prec}}^L t}{t_{\text{orb}}^2} \right)^{1/2}, \quad t \gg t_{\text{prec}}^L. \quad (18)$$

The relaxation time, defined by  $(|\Delta L_z|/L_{\max})_{\text{res}} \sim (t/t_{\text{rel}}^{\text{res}})^{1/2}$ , is then given by

$$t_{\text{rel}}^{\text{res}} \sim \frac{N}{\mu^2} \frac{t_{\text{orb}}^2}{t_{\text{prec}}^L}, \quad (19)$$

which is shorter than  $t_{\text{rel}}^{\text{nr}}$  by a factor  $(t_{\text{orb}}/t_{\text{prec}}^L) \ln \Lambda$ .

The vector angular momentum also diffuses from non-resonant relaxation, at a rate (cf. eq. [4])

$$(|\Delta \mathbf{L}|/L_{\max})_{\text{nr}} \sim \mu \frac{\eta_v}{N^{1/2}} (t/t_{\text{orb}})^{1/2}, \quad (20)$$

where  $\eta_v$  is a dimensionless constant that equals the square root of the Coulomb logarithm to within a factor of order unity.

### 1.5. Resonant Relaxation in Regular Potentials

Motion in any time-independent, regular potential can be described by action-angle variables  $(J_i, \phi_i)$  and a Hamiltonian  $\overline{H}(\mathbf{J})$ . For spherical potentials the actions  $(J_1, J_2, J_3)$  can be chosen to be, respectively, the radial action, the total angular momentum, and the  $z$ -component of the angular momentum (e.g., Tremaine & Weinberg 1984). The motion is quasiperiodic with fundamental frequencies  $\dot{\phi}_i = \Omega_i(\mathbf{J}) = \partial\overline{H}/\partial J_i$ . In a spherical potential,  $\Omega_1$  is the radial frequency,  $\Omega_2$  is the azimuthal frequency, and  $\Omega_3 = 0$ ; in a Kepler potential  $\Omega_1 = \Omega_2$ . Resonant relaxation can be important if the resonance condition  $\sum_{i=1}^3 k_i \Omega_i = 0$  is approximately satisfied for most stars, where the  $k_i$ 's are small integers with no common factor (e.g.,  $k_1 = k_2 = 0$  for a spherical potential;  $k_1 = -k_2$  for a Kepler potential).

To isolate the effects of resonant relaxation we perform a canonical transformation to new action-angle variables  $(K_i, \psi_i)$  defined by the generating function

$$S(K_i, \phi_i) = K_1 \sum_{i=1}^3 k_i \phi_i + K_2 \phi_2 + K_3 \phi_3. \quad (21)$$

Then

$$J_1 = k_1 K_1, \quad J_2 = k_2 K_1 + K_2, \quad J_3 = k_3 K_1 + K_3, \quad (22)$$

and

$$\psi_1 = \sum_{i=1}^3 k_i \phi_i, \quad \psi_2 = \phi_2, \quad \psi_3 = \phi_3. \quad (23)$$

The resonance condition implies that  $\psi_1$  is slowly varying; the effects of resonant relaxation are therefore described by a fluctuating Hamiltonian of the form  $h(\mathbf{K}, \psi_1)$ . The resonant Hamiltonian does not depend on the non-resonant angles  $\psi_2$  and  $\psi_3$  or on the time, so Hamilton's equations imply that the conjugate momenta  $K_2$  and  $K_3$  and the total energy  $E = \overline{H} + h$  are unaffected by resonant relaxation; this in turn implies that the changes in the energy and actions caused by resonant relaxation satisfy the constraints

$$\Delta E = 0, \quad \Delta \mathbf{J} = C(t) \mathbf{k}, \quad (24)$$

where  $C(t)$  is scalar.

Resonant relaxation leads to diffusion of  $C(t)$  which is described by analogs of equations (15) and (18),

$$(\Delta C/L_{\max})_{\text{res}} \sim \mu \frac{\gamma}{N^{1/2}} (t/t_{\text{orb}}), \quad t \ll t_{\text{prec}}^{\mathbf{k}};$$



$$(\Delta C/L_{\max})_{\text{res}} \sim \mu \frac{\gamma}{N^{1/2}} \left( \frac{t_{\text{prec}}^{\mathbf{k}} t}{t_{\text{orb}}^2} \right)^{1/2}, \quad t \gg t_{\text{prec}}^{\mathbf{k}}, \quad (25)$$

where  $\gamma$  is a dimensionless constant of order unity,  $\mu$  is defined in equation (16),  $t_{\text{prec}}^{\mathbf{k}} \sim (\sum k_i \Omega_i)^{-1}$  is the time required for the slow angle  $\psi_1$  to change by one radian, and we have assumed that  $|\mathbf{k}|$  is small.

### 1.6. Resonant Friction

Chandrasekhar (1943) showed that the stochastic changes in velocity associated with relaxation are accompanied by a systematic drag which he named “dynamical friction.” For massive objects (MOs) orbiting in a stellar system, orbital evolution from dynamical friction is much faster than evolution from stochastic relaxation. Near-resonances can enhance dynamical friction just as they enhance stochastic relaxation, leading to an effect we may call “resonant friction.”

To analyze resonant friction we use the formalism developed by Lynden-Bell & Kalnajs (1972); the  $z$ -component of the specific torque on the MO from dynamical friction is (Tremaine & Weinberg 1984, eq. 65)

$$T_z = 4\pi^4 m_0 \sum_{\mathbf{k}, k_3 \geq 0} k_3 \int d\mathbf{J} \sum_i k_i \frac{\partial f}{\partial J_i} |\Psi_{\mathbf{k}}|^2 \delta(\mathbf{k} \cdot \boldsymbol{\Omega} - \omega_{\mathbf{k}}). \quad (26)$$

Here  $m_0 \gg m$  is the mass of the MO,  $f(\mathbf{J})$  is the phase-space density of bound stars, and the potential of the MO has been written in the form

$$U(\mathbf{r}, t) = m_0 \text{Re} \left\{ \sum_{\mathbf{k}, k_3 \geq 0} \Psi_{\mathbf{k}}(\mathbf{J}) \exp[i(\mathbf{k} \cdot \boldsymbol{\phi} - \omega_{\mathbf{k}} t)] \right\}. \quad (27)$$

Equation (26) contains both resonant and non-resonant contributions to dynamical friction.

Now let us assume that the stellar system is spherically symmetric and that the distribution function depends only on energy and angular momentum,  $f = f(E, L)$ , consistent with Jeans’ theorem. Without loss of generality we may assume that  $z = 0$  is the orbital plane of the MO, so that the total specific torque on the MO is  $T = T_z$ . Using  $\partial E / \partial J_i = \partial \bar{H} / \partial J_i = \Omega_i$  and  $L = J_2$  we have

$$T = 4\pi^4 m_0 \sum_{\mathbf{k}, k_3 \geq 0} k_3 \int d\mathbf{J} \left( \omega_{\mathbf{k}} \frac{\partial f}{\partial E} + k_2 \frac{\partial f}{\partial L} \right) |\Psi_{\mathbf{k}}|^2 \delta(\mathbf{k} \cdot \boldsymbol{\Omega} - \omega_{\mathbf{k}}). \quad (28)$$

Now suppose that there is a near-resonance for the triplet  $\mathbf{k}_r$ . Formally, we set  $\mathbf{k}_r \cdot \boldsymbol{\Omega} = \epsilon \mathbf{k}_r \cdot \tilde{\boldsymbol{\Omega}}$  and  $\omega_{\mathbf{k}_r} = \epsilon \tilde{\omega}_{\mathbf{k}_r}$  and let  $\epsilon \rightarrow 0$ . Keeping only the largest terms in (28) gives the contribution of the triplet  $\mathbf{k}_r$  to the specific torque from resonant friction,

$$T = \frac{4\pi^4 m_0}{\epsilon} k_{3,r} k_{2,r} \int d\mathbf{J} \frac{\partial f}{\partial L} |\Psi_{\mathbf{k}_r}|^2 \delta(\mathbf{k}_r \cdot \tilde{\boldsymbol{\Omega}} - \tilde{\omega}_{\mathbf{k}_r}), \quad (29)$$

which diverges as  $\epsilon \rightarrow 0$ .

Evaluating expressions such as (29) is arduous, mostly because of the complexity of the action-angle expansion  $\Psi_{\mathbf{k}}$  of the potential of a point mass (Weinberg 1986; see also Hernquist & Weinberg 1989). However, it is simple to derive some qualitative effects of resonant friction:

- Equation (29) shows that there is no resonant friction when the distribution function is isotropic ( $\partial f / \partial L = 0$ ). The term  $\propto \partial f / \partial E$  in equation (28) contributes only non-resonant friction.
- The resonant torque is zero if the stars are on circular orbits (in this case  $\Psi_{\mathbf{k}} = 0$  unless  $k_1 = 0$ , and if  $k_1 = 0$  then resonance requires  $k_2 = 0$  since  $\Omega_2 \neq 0$  and  $\Omega_3 = 0$ ); similarly, the resonant torque is zero if the MO is on a circular orbit.
- The orbits that contribute most to the friction are those with near-zero inclinations, since these remain closest to the zero-inclination orbit of the MO and precess in the same direction. Zero-inclination orbits have  $\Psi_{\mathbf{k}} = 0$  unless  $k_2 = k_3$  (Weinberg & Tremaine 1984). Together with equation (29), this suggests that the dominant contribution to the resonant torque comes from terms with  $k_{3,r} k_{2,r} > 0$ , which in turn implies that the sign of the torque on the MO is the sign of  $\partial f / \partial L$ . In the common case where orbits are predominantly radial,  $\partial f / \partial L < 0$ , resonant friction removes angular momentum from the MO orbit at constant energy, thereby increasing its eccentricity. This effect can dominate the eccentricity evolution of black-hole binaries in galactic nuclei and may promote the merger of binary black holes, since emission of gravitational radiation is more efficient for an eccentric binary (Begelman et al. 1980, Quinlan 1996).
- The rate of growth or decay of angular momentum of the MO through resonant friction is approximately given by

$$\frac{1}{L_{\max}} \left( \frac{dL}{dt} \right)_{\text{res}} \sim \frac{T}{L_{\max}} \sim \pm \frac{m_0 M_\star}{M^2} \frac{t_{\text{prec}}^{\mathbf{k}}}{t_{\text{orb}}^2}, \quad (30)$$

where we have assumed that the orbit of the MO has moderate eccentricity and that  $|\partial f/\partial L| \sim f/L_{\max}$ . In a near-Kepler potential, where  $\mathbf{k}_r = (1, -1, 0)$  and  $t_{\text{prec}}^{\mathbf{k}}$  is given by equation (1), we have

$$\frac{1}{L_{\max}} \left( \frac{dL}{dt} \right)_{\text{res}} \sim \pm \frac{m_0}{M} \frac{1}{t_{\text{orb}}}. \quad (31)$$

In this case the frictional torque is—remarkably—-independent of the number of stars, although equation (31) holds only when  $m_0 \lesssim M_*$ . When  $m_0 \gtrsim M_*$  the precession time is  $t_{\text{prec}} \sim (M/m_0)t_{\text{orb}}$ , so that

$$\frac{1}{L_{\max}} \left( \frac{dL}{dt} \right)_{\text{res}} \sim \pm \frac{M_*}{M} \frac{1}{t_{\text{orb}}}. \quad (32)$$

The two expressions (31) and (32) can be combined,

$$\frac{1}{L_{\max}} \left( \frac{dL}{dt} \right)_{\text{res}} \sim \pm \frac{\min(M_*, m_0)}{M} \frac{1}{t_{\text{orb}}}. \quad (33)$$

For comparison, non-resonant dynamical friction removes energy and angular momentum at the slower rate

$$\frac{1}{E} \left( \frac{dE}{dt} \right)_{\text{nr}} \sim \frac{1}{L_{\max}} \left( \frac{dL}{dt} \right)_{\text{nr}} \sim -\frac{m_0 M_*}{M^2} \frac{1}{t_{\text{orb}}}. \quad (34)$$

Another manifestation of resonant friction occurs when the potential is nearly spherical but the mean rotation of the stars is non-zero (for example a stellar disk) and the orbit of the MO is inclined. In this case the distribution function  $f = f(E, L, L_z)$  depends not just on  $E$  and  $L$  but also on the  $z$ -component of angular momentum  $L_z = J_3$ . Because the potential is nearly spherical,  $\Omega_3 \simeq 0$  (i.e. inclined orbits precess slowly) so terms with  $k_1 = k_2 = 0$  are near-resonant. The  $z$ -component of the torque on an MO from the triplets  $\mathbf{k} = (0, 0, k_3)$  is

$$T_z = 4\pi^4 m_0 \sum_{k_3 \geq 0} k_3^2 \int d\mathbf{J} \frac{\partial f}{\partial L_z} |\Psi_{0,0,k_3}|^2 \delta(k_3 \Omega_3 - \omega_{0,0,k_3}). \quad (35)$$

If the stellar system rotates in a prograde direction, then  $\partial f/\partial L_z$  is generally positive so  $T_z$  is positive; thus the resonant friction erodes the inclination of the MO until it settles into the equatorial plane of the stellar system. The resonant torque is zero if the stars have precisely zero inclination (for zero-inclination stars  $\Psi_{0,0,k_3} = 0$  unless  $k_3 = 0$ ); the rate of change of the orbital inclination  $I_0$  of the MO is given approximately by

$$\frac{1}{I_0} \left( \frac{dI_0}{dt} \right)_{\text{res}} \sim \pm \frac{M_* m_0}{M^2} \frac{t_{\text{prec}}}{t_{\text{orb}}^2} \langle I^2 \rangle, \quad (36)$$

where  $\langle I^2 \rangle$  is the mean-square inclination in the disk and we have assumed  $|\partial f/\partial L_z| \sim f/L_{\max}$ .

## 2. Numerical Simulations

### 2.1. Methods

Our numerical investigation of resonant relaxation utilized two complementary approaches: an  $N$ -body code that integrates the orbits of individual stars with timestep  $\ll t_{\text{orb}}$ , and an “ $N$ -wire” code that follows the evolution of Kepler ellipses with timestep  $\ll t_{\text{prec}}$ . The  $N$ -body code allows us to follow the growth of  $\Delta E(t)$ ,  $\Delta L(t)$ , and  $\Delta \mathbf{L}(t)$  for each star; the  $N$ -wire code involves a degree of abstraction from the original problem and does not yield  $\Delta E(t)$ , but potentially allows  $\Delta L(t)$  and  $\Delta \mathbf{L}(t)$  to be followed for much longer times.

**N-body simulations** These simulations are challenging because isolating the effects of resonant relaxation requires following the  $N$ -body system for very long times (our simulations ran for up to  $10^6 t_{\text{orb}}$ ).

The  $N$ -body system contained three components:

- A fixed spherical potential,  $\Phi(r)$ . To measure the importance of resonant relaxation we compared the evolution of pairs of systems that were identical except for the fixed potentials. One potential was Keplerian,  $\Phi(r) = -GM/r$ , in which there is no orbital precession, and the other was an isochrone potential,  $\Phi(r) = -GM/[b + (b^2 + r^2)^{1/2}]$  (Hénon 1959), where  $b$  is a “core” radius, in which the precession time is comparable to the orbital period for  $r \sim b$ . We used units in which  $G = M = b = 1$ .
- $N$  identical “background” stars of mass  $m$ , which felt only the gravitational force from the fixed potential, not from each other or from the test stars. The total mass of the background stars was much smaller than the mass associated with the fixed potential; typically  $M_*/M \sim 10^{-2}$ – $10^{-5}$ .
- $n \ll N$  identical “test” stars of mass  $m$ , which felt the gravitational force from the central potential, the background stars, and from one another. (We also conducted a few simulations using test stars of unequal masses.) The use of separate background and test stars reduces the force calculation to  $O(nN)$  rather than the much larger  $O(N^2)$  for the fully self-consistent calculation; typically,  $n/N \lesssim 0.1$ .

To reduce integration errors during close encounters, the gravitational force between stars was softened. The softening length was usually  $\sim 1\%$  of the system size; the influence of softening on the results is discussed in § 2.2.

The initial distribution function of the stars was isotropic, with  $dN(E)/dE \propto E^{-2}$  for  $E_{\min} < E < E_{\max} = 10E_{\min}$  and zero otherwise. For the isochrone potential,  $|E_{\min}| = 0.05 GM/b$ ; this implies a stellar density  $\rho(r) \propto r^{-2}$  for  $b \lesssim r \lesssim 10b$ . For the Kepler potential,  $E_{\min}$  was chosen so that the typical star had the same orbital period as in the isochrone potential. Test stars were chosen such that their orbits remained within the body of the cluster, so as to avoid edge effects due to the cluster’s finite radial extent; in practice this meant limiting possible test stars to orbits that were not too eccentric,  $e \lesssim 0.8$ . For example, in the isochrone potential test stars were required to have turning points  $r_{\min} > 0.8b$  and  $r_{\max} < 9b$ , implying  $e < 0.84$ ; background stars were present in the larger region  $0.2b < r < 20b$ .

The integration algorithm was symplectic to eliminate spurious dissipation over the long integration times. We used either a second-order scheme (“leapfrog”) or its fourth-order generalization<sup>1</sup>, depending on the situation—the higher-order scheme was more accurate but the lower-order scheme was more robust during close encounters. An additional advantage of these algorithms is that they exactly conserve angular momentum when integrating motion in a central potential.

The advantages of symplectic schemes are generally lost if the timestep is varied. Thus each orbit was integrated with a fixed timestep. However, because of the wide range of orbital periods, it was useful to allow different timesteps for different orbits. To avoid having to interpolate when computing forces, the different timesteps must be commensurate; in the case of second-order leapfrog, this is easily arranged. Suppose that a timestep less than  $h_i$  is needed to maintain the desired accuracy for star  $i$ , and let  $h = \min_i h_i$ . In a leapfrog scheme with step  $h$  the forces are evaluated at times  $(k + \frac{1}{2})h$ ,  $k = 0, 1, 2, \dots$ , that is, in the middle of the timestep. Therefore we can ensure that the timesteps are commensurate by choosing timesteps  $h'_i$ , where  $h'_i$  is the largest odd multiple of  $h$  less than  $h_i$ . The further restriction that  $h'_i/h$  be a multiple of 3 ensures that all of the timesteps end at the same time as the largest timestep, making synchronized output easy. Using this approach speeded up the  $N$ -body code by a factor  $\sim 2$ – $3$ . In the fourth-order scheme, however, forces are computed at irrational (and hence unalignable) fractions of the interval, so that in this case the same timestep  $h$  was used for all stars; for fractional energy accuracies  $\epsilon \lesssim 3 \times 10^{-5}$ , the savings of the fourth-order scheme outweighed the cost of a single timestep and produced the faster code.

---

<sup>1</sup>The leapfrog map with timestep  $h$  is  $H_2(h) : (\mathbf{r}, \mathbf{v}) \rightarrow (\mathbf{r}', \mathbf{v}')$ , where  $\mathbf{r}_1 = \mathbf{r} + \frac{1}{2}h\mathbf{v}$ ,  $\mathbf{v}' = \mathbf{v} - h\nabla U(\mathbf{r}_1)$ ,  $\mathbf{r}' = \mathbf{r}_1 + \frac{1}{2}h\mathbf{v}'$ ; the fourth-order map (e.g., Yoshida 1990) is the composition of three leapfrog steps,  $H_4(h) = H_2(ah)H_2(bh)H_2(ah)$ , where  $a = 1/(2 - 2^{1/3})$  and  $b = 1 - 2a = -2^{1/3}/(2 - 2^{1/3})$ .

The size of the timestep (in units of the radial orbital period) required to maintain relative energy accuracy  $\epsilon$  was  $h \approx (r_{\min}/r_{\max})^{1.25}\epsilon^{1/2}$  for the second-order scheme and  $h \approx 0.5(r_{\min}/r_{\max})^{1.25}\epsilon^{1/4}$  for the fourth-order scheme, where  $r_{\min}$  and  $r_{\max}$  are the orbit’s turning points ( $\epsilon$  is the amplitude of the spurious energy oscillation caused by the integration algorithm; there is no systematic energy drift, because the algorithm is symplectic.). A useful check on the accuracy of the code is to follow a cluster whose background stars are artificially held fixed at their initial positions; since the test stars are then orbiting in a fixed (albeit non-spherical) potential, their orbital energy should be conserved. This test was mainly used to ensure that the error accumulated during close encounters was negligible. A second constraint on the required accuracy is that the natural orbital precession should not be artificially accelerated by integration errors. The simulations generally used  $\epsilon = 10^{-6}$ .

**N-wire simulations** The heart of these simulations is an efficient algorithm to compute the time-averaged torque between two Kepler orbits, which was supplied to us by Jihad Touma (Touma & Tremaine 1996). The evolving angular momentum for each test star was computed by straightforward integration of the time-dependent torque on the orbits using a standard (non-symplectic) adaptive ODE integrator.

The initial conditions and the division into test and background stars were the same as in the  $N$ -body code. Of course, since the analysis assumes that the orbits are approximately Keplerian, comparative integrations in the isochrone potential were not possible. The simulations also do not yield estimates for  $\Delta E$ , which is zero in this approximation. The potential advantages of the  $N$ -wire simulations are that (i) they provide an independent check on the  $N$ -body code; (ii) they isolate the effects of resonant relaxation without additional “noise” from non-resonant relaxation; (iii) the evolution of  $\Delta L$  and  $\Delta \mathbf{L}$  can be traced for longer times than in the  $N$ -body code, due to the larger timesteps that can be used (but see below).

## 2.2. Simulation Results

A sample pair of simulations illustrating the presence of resonant relaxation is shown in Figures 1 and 2, which show simulations in the Kepler and isochrone potentials respectively; we expect resonant relaxation to be important in the former case and not the latter. Both simulations used  $n = 4$  test stars out of  $n + N = 64$  total stars, each of mass  $m = 3 \times 10^{-7}M$ . (Although the total number of stars in each cluster was small, the results they display are consistent with those from larger simulations; in visual terms the small- $N$  runs show the effects of resonant relaxation most clearly since they can be evolved longer.)

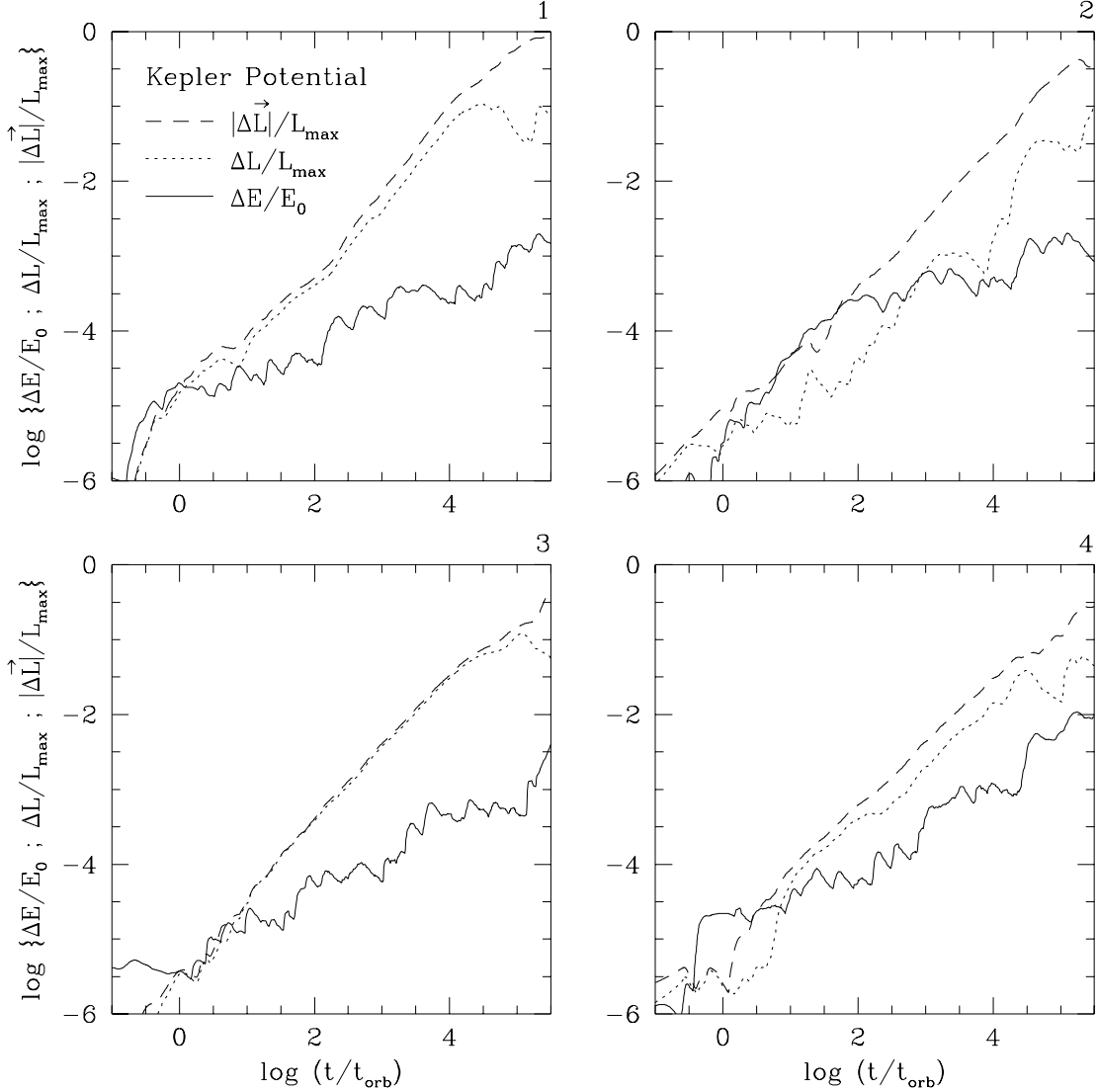


Fig. 1.— Energy and angular momentum relaxation over time (in units of the mean orbital time,  $t_{\text{orb}}$ ) for four test stars in a Keplerian star cluster. Resonant relaxation causes  $\Delta L$  (dotted line) and  $|\Delta L|$  (dashed line) to grow almost linearly with time, in contrast to the square-root growth of  $\Delta E$  (solid line), which is consistent with a random walk. Note the (weak) evidence for a turnover in the  $\Delta L$  curves at  $t \sim t_{\text{prec}} \approx 10^{4.7} t_{\text{orb}}$ , where resonant relaxation is expected to become a random walk (see eqs. 6 and 8).

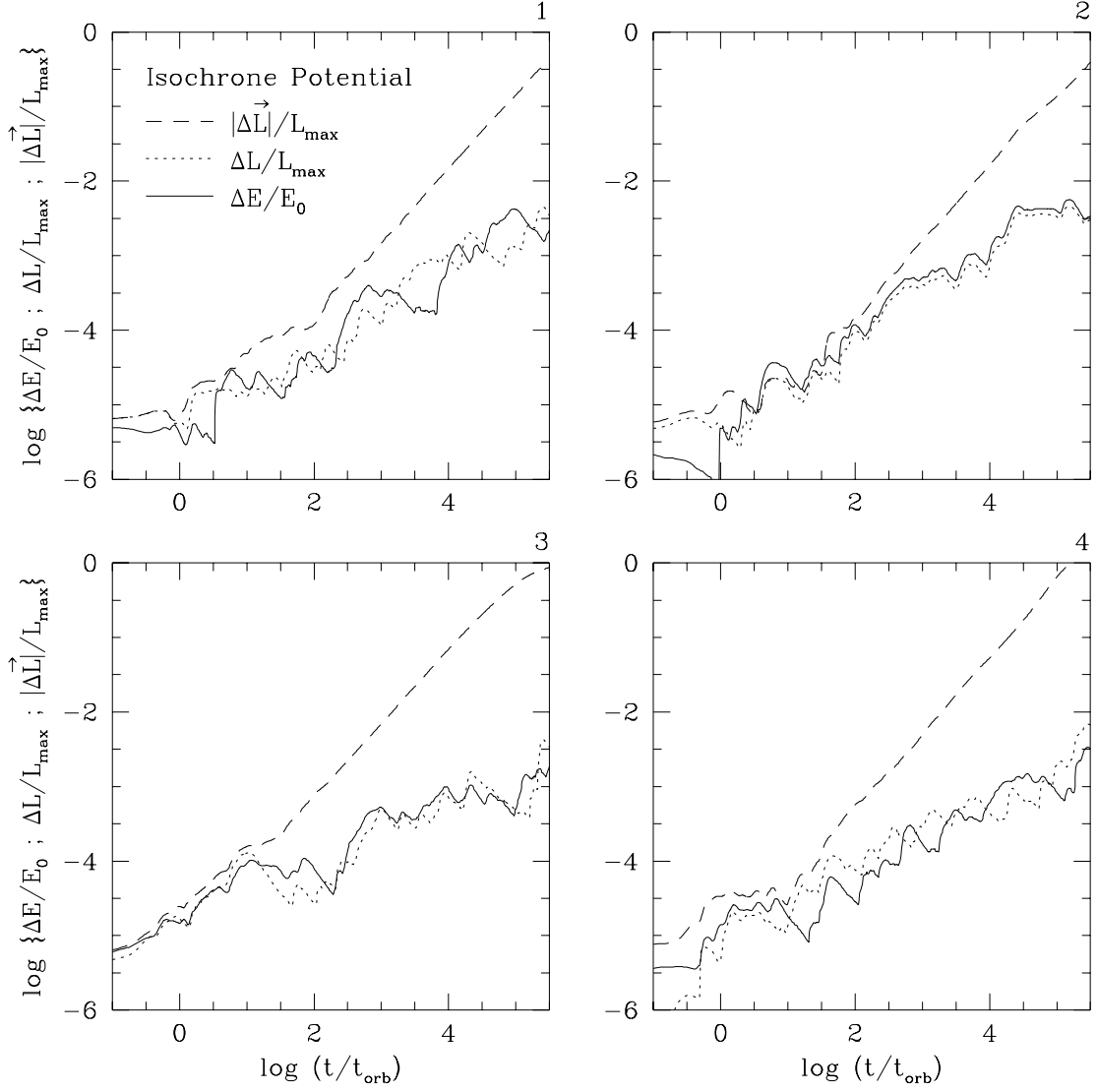


Fig. 2.— As Figure 1 but for an isochrone potential, in which there is rapid precession. Note that in this case  $\Delta L/L \sim \Delta E/E \propto t^{1/2}$  at all times; because the isochrone potential is spherical, however, resonant relaxation is present in  $|\Delta \mathbf{L}|$  (§ 1.4).



The four panels in each of Figures 1 and 2 plot the three quantities  $\Delta E/E_0$ ,  $\Delta L/L_{\max}$ , and  $|\Delta \mathbf{L}|/L_{\max}$  for the four test stars, where  $E_0$  is the initial energy and

$$L_{\max}(E) = \begin{cases} GM/(2|E|)^{1/2}, & \text{Kepler potential;} \\ GM/(2|E|)^{1/2}(1 - 2b|E|/GM), & \text{isochrone potential,} \end{cases} \quad (37)$$

is the angular momentum of a circular orbit with energy  $E$ . The times are given in units of  $t_{\text{orb}}$ , defined as the mean radial orbital period of all stars in the cluster. The difference between the two potentials is clear: in the Kepler case (Fig. 1), growth of  $\Delta L$  systematically outpaces that of  $\Delta E$ , by 1–2 orders of magnitude in the course of the integration, whereas in the isochrone potential (Fig. 2)  $\Delta L/L_{\max} \sim \Delta E/E$  at all times. In other words, if we define the (scalar) angular momentum relaxation time  $t_L$  by  $\Delta L(t_L) \sim L_{\max}(E_0)$  and the energy relaxation time  $t_E$  by  $\Delta E(t_E) \sim E_0$ , then  $t_L \ll t_E$  when precession is slow, while  $t_L \sim t_E$  otherwise. In both potentials, the vector angular momentum relaxation time  $t_{\mathbf{L}} \ll t_E$  (cf. § 1.4); however, this rapid relaxation of  $\mathbf{L}$  is less interesting since it reflects changes in the orientation rather than the shape of the orbit, which are of little consequence in non-rotating spherical clusters.

Note that for these simulations,  $t_{\text{prec}}/t_{\text{orb}} \sim M/M_{\star} \approx 10^{4.7}$ , so the figures mostly illustrate the regime  $t \ll t_{\text{prec}}$  in which  $\Delta L$  is expected to increase linearly with time (eq. 6). At times  $t \gg t_{\text{prec}}$ ,  $\Delta L$  should increase as the square root of the time (eq. 8). There is a suggestion of such a turnover in Figure 1; we comment further on this issue below.

We may test the analytic analysis of § 1 in more detail by performing least-squares fits on the simulation data. We fit each of the curves in Figures 1 and 2—and analogous curves for other simulations—to the variety of power laws, sums of power laws, and broken power laws defined in Table 1. Formula (a) tests whether  $\Delta E(t)$  exhibits the  $t^{1/2}$  dependence predicted by equation (4), and formula (b) finds the best-fit value of the parameter  $\alpha$

Table 1. Parametric Relaxation Curve Models<sup>a</sup>

$\Delta E(\tau)/E_0$	$\Delta L(\tau)/L_{\max}$	$ \Delta \mathbf{L}(\tau) /L_{\max}$
(a) $\zeta m N^{1/2} \tau^\nu$	(c) $\gamma_s m N^{1/2} \tau^{\delta_s}$	(f) $\gamma_v m N^{1/2} \tau^{\delta_v}$
(b) $\alpha m N^{1/2} \tau^{1/2}$	(d) $\eta_s m N^{1/2} \tau^{1/2} + \beta_s m N^{1/2} \tau$	(g) $\eta_v m N^{1/2} \tau^{1/2} + \beta_v m N^{1/2} \tau$
	(e) $c \tau^{b_1} / [1 + (\tau/\tau_b)^{b_3}]^{(b_1 - b_2)/b_3}$	

<sup>a</sup>  $\tau \equiv (t/t_{\text{orb}})$ ;  $M = 1$ .

in equation (4). Formula (c) tests whether  $\Delta L(t)$  is dominated by the  $t^{1/2}$  behavior characteristic of non-resonant relaxation (eq. 4) or the linear growth characteristic of resonant relaxation when  $t \ll t_{\text{prec}}$  (eq. 6); formula (d) fits simultaneously for both resonant and non-resonant relaxation in  $\Delta L$  (eqs. 4 and 6); and formula (e) fits to a broken power law ( $\propto t^{b_1}$  for small  $t$  and  $\propto t^{b_2}$  for large  $t$ , the transition occurring at  $t/t_{\text{orb}} \sim \tau_b$ ) to look for the turnover from linear growth (eq. 6) to square-root growth (eq. 8) that is expected at  $t \sim t_{\text{prec}}$ . Finally, formulae (f) and (g) are the vector analogs of (c) and (d) (cf. eqs. 15 and 20).

In performing the fits, random noise in the relaxation curves of individual test stars is a significant concern. Note first that fitting to the raw output is undesirable because curves such as  $\Delta E(t)$  cross zero many times, which in log-log space implies passage through  $-\infty$ ; what is wanted is a fit to the more steadily growing *envelope*, ignoring the zero crossings. This was done by smoothing the individual curves using an averaging window of width  $\Delta \log t \sim 0.1$  to replace each data point by the weighted average of its neighbors, larger data points receiving greater weight (the weighting factor was proportional to the square of the data point). This window was large enough to remove the sharp “dropouts” due to zero crossings, but too small to affect the global shape of the envelope (decreasing the window size to  $\Delta \log t \sim 0.03$  changed power-law slopes by  $\lesssim 1\%$ , but noticeably increased the random noise). As these smoothed curves still contain (real!) random variations, more robust results were obtained by averaging the curves for all test stars in a particular simulation, scaled temporally by their respective orbital periods, to create composite average relaxation curves for the cluster, model parameters being calculated from these composites. Conceptually one can think of these curves as belonging to a fictitious “average” star with orbital period  $t_{\text{orb}}$ ; we will use this term to label such fits. An alternative procedure is to derive best-fit parameters for individual stars and then average these results; this method is less robust since it attempts to remove the random noise *after* performing the fits, which can be ineffective if this noise causes the fits to be poor. Therefore, all of our quantitative results are based solely on fits to the average star as defined above.

Tables 2 and 3 show derived parameter values for the relaxation curves shown in Figures 1 and 2. Fits to the individual test stars, the averages of the fit parameters (labeled mean), and fits to the average star (labeled AS) are given. Comparison of Tables 2 and 3 shows the effect of resonant relaxation quite clearly. In Table 2 (Kepler model) the exponent  $\delta_s$  for  $\Delta L/L_{\text{max}}$  (formula [c]) is near unity, corresponding to the linear growth expected for resonant relaxation; while the exponent  $\nu$  for  $\Delta E/E_0$  (formula [a]) is near 0.5, corresponding to a random walk dominated by non-resonant relaxation (recall that there is no resonant energy relaxation). On the other hand, in Table 3 (isochrone model) there is no systematic difference between the exponents  $\delta_s$  and  $\nu$ .

Table 2. Best-fit Parameters for Figure 1 (Kepler Potential)

Formula Number and Parameters							
Star	(b) $\alpha$	(a) $\zeta, \nu$	(c) $\gamma_s, \delta_s$	(f) $\gamma_v, \delta_v$	(d) $\eta_s, \beta_s$	(g) $\eta_v, \beta_v$	(e) $\log \tau_b, b_2$
1	1.73	3.8, 0.39	2.0, 0.92	2.4, 0.96	2.8, 0.92	3.2, 1.51	4.7, -0.17
2	5.40	9.9, 0.40	0.9, 0.84	3.4, 0.94	1.2, 0.22	2.5, 2.03	3.8, 1.05
3	2.31	2.9, 0.46	2.2, 1.00	2.5, 1.00	0.0, 2.50	0.0, 2.76	4.5, -0.50
4	6.36	5.2, 0.53	2.4, 0.88	5.6, 0.87	0.6, 1.17	4.0, 2.20	3.8, -0.10
mean	3.26	4.2, 0.45	2.0, 0.95	3.2, 0.95	1.9, 1.28	2.2, 2.10	4.4, 0.07
AS	3.51	5.2, 0.44	1.8, 0.90	3.5, 0.93	1.6, 0.85	2.4, 2.04	4.5, 0.18

Table 3. Best-fit Parameters for Figure 2 (Isochrone Potential)

Formula Number and Parameters							
Star	(b) $\alpha$	(a) $\zeta, \nu$	(c) $\gamma_s, \delta_s$	(f) $\gamma_v, \delta_v$	(d) $\eta_s, \beta_s$	(g) $\eta_v, \beta_v$	(e) $\log \tau_b, b_2$
1	2.36	1.7, 0.56	2.3, 0.52	2.3, 0.85	2.5, 0.00	3.7, 0.55	0.1, 0.52
2	5.06	3.0, 0.59	2.0, 0.61	1.8, 0.91	3.1, 0.01	2.1, 0.75	-0.1, 0.61
3	2.87	8.5, 0.34	7.0, 0.34	4.4, 0.89	3.4, 0.00	6.5, 1.47	0.6, 0.33
4	1.65	2.7, 0.43	3.1, 0.44	1.5, 0.95	2.3, 0.00	2.6, 0.82	0.5, 0.44
mean	2.80	3.5, 0.48	2.8, 0.50	3.0, 0.89	2.6, 0.00	4.6, 0.99	0.2, 0.49
AS	2.84	3.2, 0.48	3.1, 0.48	2.5, 0.89	2.9, 0.00	3.6, 0.84	0.5, 0.46

The difference between the Kepler and isochrone potentials is also reflected in the fits to formula (d), which decomposes the relaxation into terms  $\propto t^{1/2}$  (non-resonant) and  $\propto t$  (resonant). The strength of the resonant term, which is proportional to  $\beta_s$ , is comparable to the strength of the non-resonant term in the Kepler potential, but is essentially zero in the isochrone model.

The presence of resonant relaxation of the vector angular momentum in spherical potentials is illustrated by the exponent  $\delta_v$  for  $\Delta\mathbf{L}/L_{\max}$ , which is near unity in both Tables 2 and 3 (eq. 15).

A glance at the derived values for  $\log \tau_b$  and  $b_2$  in Table 2 illustrates the advantage of using the average star to compute parameters instead of averaging the fits to individual stars; the individual fits are so noisy that averaging after the fact is nearly meaningless. Note that  $\log \tau_b$  for the average star in Table 2 is of order the expected value,  $\log(t_{\text{prec}}/t_{\text{orb}}) \sim \log(M/M_\star) \sim 4.7$ .

We originally hoped that the  $N$ -wire code could be run for many more orbital times than the corresponding  $N$ -body calculation, since the required integration step is much longer. This hope was frustrated by close encounters of the wires, which required each wire to be divided into hundreds or even thousands of segments for accurate calculation of the torque (the calculations for each segment taking  $\sim 10^2$ – $10^3$  times longer than the simple force calculations of the  $N$ -body code). These encounters dominated the computation time, so that the  $N$ -wire code was significantly *slower* than the  $N$ -body code, particularly for larger  $N$ . Nevertheless, the  $N$ -wire simulations that were performed showed the same qualitative features as their  $N$ -body counterparts, including clear evidence of resonant relaxation of similar strength, and the suggestion of a turnover near  $t \sim t_{\text{prec}}$ . The  $N$ -wire code could be sped up in several ways: by softening the potential from the wires, by using a finer mesh close to the crossing point, or by analytic evaluation of the torque when the wires are close to crossing. However, as there appeared to be no new features in the relaxation curves, a substantial effort to improve the speed was not deemed worthwhile, and quantitative results from the wire simulations will not be given.

Table 4 lists the best-fit model parameters averaged over  $\approx 30$   $N$ -body simulations spanning several orders of magnitude in  $m$  (from  $3 \times 10^{-8}$  to  $3 \times 10^{-5}$ ) and  $N$  (from 64 to 8192). The contribution of each simulation to the average was weighted by the standard error in the fit, which in turn was determined by choosing the error for each data point in the simulation so that  $\chi^2 = 1$  per degree of freedom.

The results nicely confirm our theoretical expectations: (i) In both the Kepler and isochrone potentials, the evolution of  $\Delta E$  is consistent with a random walk, that is, the

Table 4. Global Average Best-fit Parameters<sup>a</sup>

Formula	Parameters	Kepler Potential	Isochrone Potential
(b)	$\alpha$	3.09(0.11) [0.25]	2.76(0.11) [0.23]
(a)	$\zeta, \nu$	3.24(0.17), 0.49(0.01) [0.23]	2.93(0.18), 0.49(0.01) [0.21]
(c)	$\gamma_s, \delta_s$	1.35(0.08), 0.85(0.02) [0.26]	2.87(0.12), 0.49(0.01) [0.21]
(f)	$\gamma_v, \delta_v$	2.78(0.18), 0.88(0.01) [0.17]	2.73(0.15), 0.84(0.02) [0.33]
(d)	$\eta_s, \beta_s$	1.37(0.11), 0.53(0.06) [0.22]	2.76(0.09), 0.00(0.01) [0.24]
(g)	$\eta_v, \beta_v$	2.08(0.26), 1.79(0.12) [0.11]	3.50(0.10), 0.71(0.07) [0.13]
(e)	$\log \tau_b, b_2$	0.02(0.27) <sup>b</sup> , 0.49(0.13) [0.04]	0.73(0.14), 0.49(0.01) [0.04]

<sup>a</sup> The numbers in parentheses are 1- $\sigma$  errors on the best-fit parameters, which were derived by assuming equal error (in dex) for each simulation data point and choosing this error so that  $\chi^2 = 1$  per degree of freedom (the required errors in the data points in dex are given in square brackets).

<sup>b</sup> This number is  $\log(\tau_b/\tau_{\text{prec}})$ , not  $\log \tau_b$ .

exponent  $\nu = 0.5$  to within the errors; moreover, the rate of energy relaxation is nearly identical in the two models (the values for  $\alpha$  differ by only 10%), which confirms that they are close analogs except for the resonance in the Kepler case. (ii) In the isochrone potential, the evolution of  $\Delta L$  is consistent with a random walk, that is,  $\delta_s = 0.5$  to within the errors; while in the Kepler case  $\Delta L$  grows much more rapidly (the derived value  $\delta_s = 0.85 \pm 0.02$  is less than the expected value of 1, presumably because small-scale fluctuations in the torque add a random-walk component—this issue is discussed further below). There is also no evidence for a linear component in  $\Delta L$  in the isochrone model ( $\beta_s = 0$ ). (iii) The growth of  $\Delta \mathbf{L}$  is more rapid than a random walk in both potentials; once again, the derived values  $\delta_v = 0.88 \pm 0.01, 0.84 \pm 0.02$  are lower than unity because of small-scale fluctuations in the torque. (iv) The value of  $\tau_b$  is close to the expected value  $\tau_{\text{prec}}$  in the Kepler potential ( $\log(\tau_b/\tau_{\text{prec}}) = 0.02 \pm 0.27$ ); moreover, as predicted by equation (8), the evolution of  $\Delta L$  for  $t \gg t_{\text{prec}}$  is consistent with a random walk (which requires  $b_2 = 0.5$ ; the observed value is  $0.49 \pm 0.13$ ).

Note that the diffusion in angular momentum, as measured by  $\eta_s$  and  $\eta_v$ , is stronger in the isochrone than the Kepler potential (perhaps because the encounter velocities are smaller in the isochrone core), while the resonant relaxation in  $\mathbf{L}$ , as measured by  $\beta_v$ , is stronger in the Kepler potential because of the contribution to the torque from the eccentricity of the orbits.

We now comment on whether the linear/random-walk model (formulae [d] and [g]) provides a better fit to  $\Delta L$  and  $\Delta \mathbf{L}$  than a simple power-law (formulae [c] and [f]). Table 4 shows that in all three cases of interest (Kepler  $\Delta L$  and  $\Delta \mathbf{L}$ , and isochrone  $\Delta \mathbf{L}$ ) formula (d) fits better than (c) and (g) fits better than (f), the required errors in the data points to achieve a given  $\chi^2$  being smaller. To determine whether this difference is significant, paired sample Student’s t-tests were performed to compute the confidence level at which the hypothesis of the corresponding  $\chi^2$  values having the same mean could be excluded. For both potential models, the resulting confidence for  $\Delta \mathbf{L}$  was over 99.9%—the power-law model is clearly inferior to the linear/random-walk model. In the case of  $\Delta L$  (Kepler potential), applying the t-test to the full simulation set gave a confidence of only  $\approx 85\%$  that the linear/random-walk model provides a better fit; this weaker result is not surprising since the relaxation curves are noisier. By performing the test using only the 6 simulations with at least 32 test stars, we obtained a stronger confidence level of  $\approx 95\%$ .

We also checked the scaling of the relaxation rate with  $m$  and  $N$ , by fitting the simulations to a formula of the form  $\Delta E/E_0 = \alpha m^a N^b \tau^{1/2}$ ; this gave  $\alpha = 3.6 \pm 0.9$ ,  $a = 1.02 \pm 0.01$ , and  $b = 0.51 \pm 0.03$ . Thus the exponents are consistent with their predicted values  $a = 1, b = \frac{1}{2}$  to within a few percent. Similar results were obtained from fits to  $\Delta L$

and  $\Delta L$ .

We note that softening is expected to affect the strength of the random walk terms in the simulations by changing the value of the “ $\ln \Lambda$ ” factor which these terms implicitly contain. In general, one expects  $\Lambda \sim R/\max(s, GM/v^2)$ , where  $s$  is the softening length and  $R$  the system size. Since  $s \gg GM/v^2$  in all of our simulations, we expect that  $\alpha^2 \propto t_E^{-1} \propto \ln[K(R/s)]$  for some factor  $K \sim 1$ . To test this scaling, we ran a series of Kepler simulations in which the softening length was reduced by a factor of 100 (from  $s \simeq 10^{-2} R$  to  $s \simeq 10^{-4} R$ ), which should increase  $\alpha$  by a factor of about 1.4. It was found that  $\alpha = 5.5 \pm 0.2$  for these runs, a factor of 1.8 larger than in Table 4, which is in line with expectations given the uncertainties. Similar increases were seen in other parameters, such as  $\eta_s$  which increased by a factor of 1.6. This observation also supports our claim that the  $\eta$  parameter really is measuring a random-walk component in  $\Delta L$ .

### 3. Implications for Galactic Nuclei

#### 3.1. Black Hole Fueling Rates

Tidally disrupted stars can be an important fuel source for massive black holes in stellar systems, disruption occurring if the stars pass closer to the black hole than their tidal radius,  $r_t$ . The pericenter of an orbit with energy  $E \gg -GM/r_t$  is within the tidal radius if its angular momentum is less than  $L_{\min} \simeq (2GM r_t)^{1/2}$ ; the region in phase space  $L < L_{\min}$  is known as the “loss cone” because stars in this region will be disrupted in less than one orbital period, unless their orbits are perturbed out of the loss cone before reaching pericenter. Angular momentum relaxation provides a steady supply of stars to the loss cone. This mass supply rate is interesting in the context of active galactic nuclei (AGNs), for which tidal disruption of stars is a possible fueling mechanism. Previous studies (e.g., Duncan & Shapiro 1983; David et al. 1987a,b; Murphy et al. 1991; Polnarev & Rees 1994) concluded that (non-resonant) relaxation is too slow to sustain typical AGN luminosities, unless mass loss is dominated by other mechanisms (such as physical collisions between stars) or additional, large-scale torques are present (as from a nuclear bar, binary black hole, or triaxial galactic potential). In this section we investigate whether resonant relaxation can enhance the supply of stars to the loss cone and hence the fueling rate of AGNs from disrupted stars.

We shall parameterize the loss rate of stars by the dimensionless number  $\lambda(E)$ , which is the fraction of stars at a given energy that are disrupted each orbital period. Let  $\Delta L_{\text{orb}}$  be the root-mean-square change in scalar angular momentum in one orbital period. For

non-resonant relaxation, equation (4) implies

$$\frac{\Delta L_{\text{orb}}^{\text{nr}}}{L_{\text{max}}} \sim \eta_s \frac{mN^{1/2}}{M}, \quad (38)$$

while for resonant relaxation, equation (6) implies

$$\frac{\Delta L_{\text{orb}}^{\text{res}}}{L_{\text{max}}} \sim \beta_s \frac{mN^{1/2}}{M}; \quad (39)$$

the non-resonant contribution to  $\Delta L_{\text{orb}}$  is stronger by of order the square root of the Coulomb logarithm. Lightman & Shapiro (1977) distinguish two cases: the “pinhole” limit in which  $\Delta L_{\text{orb}} \gg L_{\text{min}}$ , and the “diffusion” limit in which  $\Delta L_{\text{orb}} \ll L_{\text{min}}$ . First consider the pinhole limit. Here leakage of stars into the loss cone is too small to affect the distribution function significantly, so that the distribution function is approximately uniform on the energy surface in phase space, even near the loss cone. Hence the fraction of stars at a given energy that is lost per orbital period is simply the fractional area in the energy surface occupied by the loss cone,

$$\lambda(E) \simeq \frac{L_{\text{min}}^2}{L_{\text{max}}^2(E)} \quad (\Delta L_{\text{orb}} \gtrsim L_{\text{min}}). \quad (40)$$

In this limit the fueling rate is independent of the strength of the relaxation, so long as  $\Delta L_{\text{orb}} \gtrsim L_{\text{min}}$ . Therefore the loss rate in this case is unaffected by resonant relaxation, since  $\Delta L_{\text{orb}}$  is dominated by non-resonant relaxation. The pinhole limit requires

$$\frac{L_{\text{min}}}{L_{\text{max}}} \lesssim \eta_s \frac{mN^{1/2}}{M}. \quad (41)$$

When “ $\lesssim$ ” is replaced by “=,” equation (41) defines the so-called critical radius,  $r_{\text{crit}}$ ; in general the pinhole limit applies outside the critical radius and the diffusion limit applies at smaller radii.

Next consider the diffusion limit. In the absence of resonant relaxation the loss rate can be determined by solving the Fokker-Planck equation (e.g., Lightman & Shapiro 1977; Cohn & Kulsrud 1978), and is found to be

$$\lambda^{\text{nr}}(E) \simeq \frac{(\Delta L_{\text{orb}}^{\text{nr}})^2}{L_{\text{max}}^2(E) \ln(L_{\text{max}}/L_{\text{min}})} \quad (\Delta L_{\text{orb}} \lesssim L_{\text{min}}). \quad (42)$$

Now assume resonant relaxation is present. Over timescales  $\ll t_{\text{prec}}$  the resonant torque is approximately constant, so the angular momentum drifts at a nearly uniform rate. Since  $t_{\text{prec}}/t_{\text{orb}} \sim M/M_\star \gg 1$  whenever resonant relaxation is important, we may assume that



$(t_{\text{prec}}/t_{\text{orb}}) \Delta L_{\text{orb}}^{\text{res}} \gg L_{\text{min}}$ , at least if we are not too far inside the critical radius. Then the evolution of the angular momentum on the scale of the loss cone resembles a steady drift rather than diffusion, so a typical area  $\sim L_{\text{min}} \Delta L_{\text{orb}}^{\text{res}}$  is swept into the loss cone per orbital period, and the loss rate is

$$\lambda^{\text{res}}(E) \sim \frac{L_{\text{min}} \Delta L_{\text{orb}}^{\text{res}}}{L_{\text{max}}^2(E)} \quad (\Delta L_{\text{orb}} \lesssim L_{\text{min}}). \quad (43)$$

The ratio of the resonant loss rate to the non-resonant loss rate in the diffusion limit is

$$\frac{\lambda^{\text{res}}}{\lambda^{\text{nr}}} \sim \frac{L_{\text{min}} \Delta L_{\text{orb}}^{\text{res}}}{(\Delta L_{\text{orb}}^{\text{nr}})^2} \ln(L_{\text{max}}/L_{\text{min}}) \quad (\Delta L_{\text{orb}} \lesssim L_{\text{min}}). \quad (44)$$

Since  $\Delta L_{\text{orb}}^{\text{res}}$  and  $\Delta L_{\text{orb}}^{\text{nr}}$  differ only by a logarithmic factor (cf. eqs. [38] and [39]), the loss rate in the diffusion limit is much larger under resonant relaxation than under non-resonant relaxation. (Note that formula [43] neglects the relativistic effects discussed in § 3.2, which reduce the resonant loss rate in galactic nuclei.) However, this enhanced loss rate does not strongly affect the total rate of fueling of the black hole by bound stars. The reason is that the overall flux of stars into the cusp—which in a steady state equals the fueling rate from bound stars—is determined by the bottleneck at the critical radius (i.e., by the slow diffusion of orbital *energies*, the rate of which is unaffected by resonant relaxation); the enhanced loss rate inside  $r_{\text{crit}}$  will reduce the density of stars at  $r < r_{\text{crit}}$  and the radial profile of the cusp of bound stars, but it will not strongly affect the overall disruption rate. We conclude that resonant relaxation does not significantly enhance the viability of tidal disruption as a possible AGN fueling mechanism.

### 3.2. Relativistic Effects

We have assumed so far that stellar orbits are Keplerian whenever the black-hole mass is much larger than the mass in stars. At small radii, however, relativistic effects cause orbits to precess rapidly, which quenches the resonant relaxation. In the present case the most important relativistic effects are the precession of periapsis and Lense-Thirring precession of the orbital plane. The former effect (observed in the solar system as a component of Mercury’s perihelion precession, for example) is present around both Schwarzschild (non-rotating) and Kerr (rotating) black holes; in both cases, the change in the argument of periapsis per orbit in the weak-field limit is given to leading order by

$$\Delta\omega \simeq \frac{6\pi(GM/c^2)}{a(1-e^2)}, \quad (45)$$

where  $M$  is the hole mass,  $a$  and  $e$  are the orbit’s semi-major axis and eccentricity, and the precession is in the direction of motion (e.g., Darwin 1961). Around a Kerr black hole—the expected case for the nuclei of AGNs, since disk accretion will spin up an initially non-rotating black hole (Bardeen 1970, Thorne 1974)—orbits also undergo Lense-Thirring precession, which in the weak-field limit appears as a precession of the orbital angular momentum vector around the black hole’s angular momentum vector. However, this effect merely adds another (uninteresting) secular growth term to  $\Delta\mathbf{L}$ , and hence is not important for the present analysis.

Let us define a relativistic precession timescale,  $t_{\text{prec}}^{\text{GR}} = [\pi/\Delta\omega]t_{\text{orb}}$ , and a non-relativistic precession timescale,  $t_{\text{prec}}^{\text{Kep}} \sim (M/M_\star)t_{\text{orb}}$  (eq. 1), where  $t_{\text{orb}}$  is the orbital period. Relativistic precession can be important only when  $t_{\text{prec}}^{\text{GR}} \lesssim t_{\text{prec}}^{\text{Kep}}$ . In fact, since the relativistic precession is prograde ( $\Delta\omega^{\text{GR}} > 0$ ) while the non-relativistic precession is generally retrograde ( $\Delta\omega^{\text{Kep}} < 0$ ), relativistic effects slightly *enhance* resonant relaxation so long as  $t_{\text{prec}}^{\text{GR}} \gtrsim t_{\text{prec}}^{\text{Kep}}$ . Even when  $t_{\text{prec}}^{\text{GR}} < t_{\text{prec}}^{\text{Kep}}$ , resonant angular momentum relaxation remains important and is described by equation (7) so long as  $t_{\text{prec}}^{\text{GR}} \gg t_{\text{orb}}$ , although the relaxation time is increased by a factor  $t_{\text{prec}}^{\text{Kep}}/t_{\text{prec}}^{\text{GR}}$ .

The angular momentum of a Kepler orbit is given by  $L^2 = GMa(1 - e^2)$ , so the relativistic precession time may be written

$$t_{\text{prec}}^{\text{GR}} = \frac{1}{6} \left( \frac{cL}{GM} \right)^2 t_{\text{orb}}. \quad (46)$$

Thus resonant relaxation is completely quenched by relativistic effects when  $L \lesssim L^{\text{GR}}$ , where  $L^{\text{GR}} = GM/c$ . A more precise statement is that there is a region of angular-momentum space in which resonant relaxation is completely quenched only if

$$L^{\text{GR}} \gtrsim \max(\Delta L_{\text{orb}}, L_{\text{min}}); \quad (47)$$

if  $L^{\text{GR}} < L_{\text{min}}$  stars are disrupted before the relativistic precession time becomes comparable to the orbital time, and if  $L^{\text{GR}} < \Delta L_{\text{orb}}$  a star can relax across the relativistic region in less than one orbit, thereby avoiding the relativistic precession (nearly all of which occurs at periapsis). If the inequality (47) is satisfied, the angular momentum diffuses through resonant relaxation when  $L \gtrsim L^{\text{GR}}$  and by non-resonant relaxation when  $L_{\text{min}} + \Delta L_{\text{orb}} \lesssim L \lesssim L^{\text{GR}}$ ; stars will pile up in the latter region of phase space since non-resonant relaxation is slower. Even outside this region, relativistic precession can dominate the precession rate and hence reduce the rate of resonant relaxation.

The inequality (47) requires either that the loss cone is empty ( $\Delta L_{\text{orb}} \lesssim L_{\text{min}}$ ) and that  $L^{\text{GR}}/L_{\text{min}} \gtrsim 1$ , or that  $L^{\text{GR}}/\Delta L_{\text{orb}} \gtrsim 1$  if the loss cone is full; since resonant relaxation does not affect disruption rates if the loss cone is full, the latter case is uninteresting. A

numerical value for the former condition is easily derived; noting that  $L_{\min} \simeq (2GM r_t)^{1/2}$ , where  $r_t \simeq 2r_*(M/m)^{1/3}$  is the tidal radius of a star of mass  $m$  and radius  $r_*$ , assuming  $r_* \propto m^{2/3}$  (reasonable for both low and high mass main-sequence stars), and normalizing to solar values, we obtain

$$\frac{L^{\text{GR}}}{L_{\min}} \simeq 0.3 \left( \frac{M}{10^8 M_\odot} \right)^{1/3} \left( \frac{M_\odot}{m} \right)^{1/6}. \quad (48)$$

Resonant relaxation only dominates non-resonant relaxation when  $t_{\text{prec}} \gtrsim 10 t_{\text{orb}}$  (cf. eq. 52)—which here implies  $L \gtrsim 8L^{\text{GR}}$ . Therefore we may assume that relativistic precession will substantially affect the loss rate when the loss cone is empty and  $L_{\min} \lesssim 4L^{\text{GR}}$ , which implies

$$M \gtrsim 4 \times 10^7 \left( \frac{m}{M_\odot} \right)^{1/2} M_\odot. \quad (49)$$

The mass estimate (49) is quite uncertain, but lies squarely inside an interesting range: the estimated masses of black holes in galactic nuclei range from  $\sim 10^6 M_\odot$  to over  $10^9 M_\odot$ , and the Eddington luminosity corresponding to (49) is  $L_{\text{Edd}} \sim 5 \times 10^{45} \text{ erg s}^{-1}$ —a typical AGN luminosity.

To summarize, in galactic nuclei relativistic precession substantially reduces—and can even completely quench—resonant relaxation close to the loss cone. A more sophisticated treatment than the one leading to equation (43) would be required to determine the disruption rate and density profile when the loss cone is empty. Such an analysis is beyond the goals of this investigation.

### 3.3. Relaxation Time Estimates

The non-resonant relaxation time in a stellar system may be written (e.g., Binney & Tremaine 1987, eq. 8-71)

$$t_{\text{rel}}^{\text{nr}} = 0.3 \frac{\sigma^3}{G^2 m \rho \ln \Lambda}, \quad (50)$$

where  $\sigma$  is the one-dimensional velocity dispersion and  $\rho$  is the stellar density. Specializing to the case of stars in the potential of a black hole of mass  $M$ , we may write  $\sigma \simeq (GM/3r)^{1/2}$ ,  $\rho \simeq M_*/(\frac{4}{3}\pi r^3)$ , and  $\Lambda \simeq N$ ; thus

$$\begin{aligned} t_{\text{rel}}^{\text{nr}} &\simeq 0.3 \frac{M^{3/2} r^{3/2}}{G^{1/2} m^2 N \ln N} \\ &= \frac{4 \times 10^{10} \text{ yr}}{\ln N} \left( \frac{M}{M_*} \right) \left( \frac{M}{10^8 M_\odot} \right)^{1/2} \left( \frac{1 M_\odot}{m} \right) \left( \frac{r}{1 \text{ pc}} \right)^{3/2}. \end{aligned} \quad (51)$$

The resonant relaxation time (cf. §§ 1.2–1.3) is

$$t_{\text{rel}}^{\text{res}} \simeq \frac{\eta_s^2 M_\star}{\beta_s^2 M} t_{\text{rel}}^{\text{nr}} \simeq 7 \frac{M_\star}{M} t_{\text{rel}}^{\text{nr}}, \quad (52)$$

where  $\beta_s$  and  $\eta_s$  are taken from Table 4.

Table 5 applies these estimates to several nearby galaxies that are believed to harbor massive black holes (Kormendy & Richstone 1995). The table lists the resonant and non-resonant relaxation times  $t_{\text{rel}}^{\text{res}}$  and  $t_{\text{rel}}^{\text{nr}}$ , at  $0''.1$  from the center for external galaxies (roughly Hubble Space Telescope resolution) and at  $1''.0$  for the Galaxy.

We see that resonant relaxation generally does not influence the structure of galaxies ( $t_{\text{rel}}^{\text{res}} \gtrsim 10^{10}$  yr) at available resolutions, except in a few Local Group members such as M32 and the Galaxy. M31 contains a region in which  $t_{\text{rel}}^{\text{res}} < 10^{10}$  yr  $< t_{\text{rel}}^{\text{nr}}$  that is almost (!) resolvable by HST. At smaller distances from the black hole the resonant relaxation time is shorter; crude extrapolations indicate that  $t_{\text{rel}}^{\text{res}} \lesssim 10^9$  yr at radii less than  $0''.05$  in M32, at  $0''.01$  in M31, and at  $0''.002$  in NGC 3115. The first two of these could be resolved with proposed space-based interferometers.

#### 4. Discussion

Resonant relaxation is the dominant source of angular momentum relaxation for stellar systems in near-Keplerian potentials, and thus plays an important role in determining the structure of stellar cusps around black holes in galactic nuclei or globular clusters. Resonant relaxation enhances the angular momentum relaxation rate by roughly the ratio of the mass of the black hole to the mass in stars but does not affect the energy relaxation rate (more precisely, the combination of actions  $J_1 - J_2$  is conserved, where  $J_1$  is the radial action and  $J_2$  is the angular momentum).

Resonant relaxation is also present in the harmonic potentials that characterize constant-density cores, and may enhance the rate of angular momentum relaxation in the cores of globular clusters. In constant-density cores, resonant relaxation preserves the combination of actions  $J_1 - 2J_2$ . This form of resonance is not likely to be important for elliptical galaxies, which do not generally have constant-density cores (e.g., Gebhardt et al. 1996).

One might speculate that generic potentials contain (high-order) resonances that are strong enough to support resonant relaxation. In this case the angular momentum relaxation time would be much shorter than the energy relaxation time throughout most

Table 5. Characteristics of Nearby Massive Black Hole Candidates

Galaxy	$D$ (Mpc)	$M$ ( $M_{\odot}$ )	$\theta(\mu = 0.1)$ ( $''$ )	$\mu(0'.1)^a$	$t_{\text{rel}}^{\text{res}}(0'.1)^a$ (yr)	$t_{\text{rel}}^{\text{nr}}(0'.1)^a$ (yr)	$\theta_{\text{res}}$ ( $''$ )
Milky Way	0.0085	$2 \times 10^6$	6	0.001	$2 \times 10^8$	$3 \times 10^{10}$	12
M32	0.7	$2 \times 10^6$	0.08	0.2	$4 \times 10^9$	$3 \times 10^9$	0.1
M31	0.7	$3 \times 10^7$	0.5	0.002	$2 \times 10^{10}$	$1 \times 10^{12}$	0.07
NGC 3377	9.9	$8 \times 10^7$	0.05	0.3	$1 \times 10^{12}$	$3 \times 10^{11}$	0.005
NGC 3115	8.4	$2 \times 10^9$	0.5	0.02	$2 \times 10^{12}$	$2 \times 10^{13}$	0.002
M87	15.3	$3 \times 10^9$	1.3	0.001	$8 \times 10^{12}$	$1 \times 10^{15}$	0.001

<sup>a</sup>For the Galactic Center only, these values are given at  $1''.0$ , not  $0''.1$ .

Note. — Estimated distance  $D$  and black-hole mass  $M$  are from Kormendy & Richstone (1995). The quantity  $\mu(r)$  is the fraction of the total mass inside radius  $r$  that resides in stars;  $\mu \ll 1$  implies that the potential is nearly Keplerian and when  $\mu \lesssim 0.1$  resonant relaxation dominates non-resonant relaxation (eq. 52). The resonant and non-resonant relaxation times  $t_{\text{rel}}^{\text{res}}$  and  $t_{\text{rel}}^{\text{nr}}$  are given by equations (51) and (52);  $\theta_{\text{res}}$  is the apparent angular distance from the black hole at which the resonant relaxation time is  $10^{10}$  yr. Stellar density estimates for external galaxies are based on Hubble Space Telescope photometry (Faber et al. 1996) and assumed mass-to-light ratios; densities for the Milky Way are based on near-infrared photometry (Kent 1992) and an assumed core radius of 0.15 pc (Eckart et al. 1993).

of a galaxy. We suspect that this speculation is not correct, since our  $N$ -body simulations in the isochrone potential yield very similar relaxation rates for the energy and angular momentum. Nevertheless, the presence of resonant relaxation is a reminder that our understanding of relaxation in stellar systems is crude, and has not been numerically verified under conditions ( $N \sim 10^{11}$ ) found in real galaxies.

Resonant friction leads to growth or decay of the eccentricity of massive objects orbiting in near-Kepler potentials, depending on whether the star orbits are predominantly radial or tangential. Resonant friction can strongly influence the orbital evolution of a binary black hole (at least if the mass ratio of the binary is sufficiently far from unity). In radially biased star clusters the eccentricity of the binary will grow, at a rate faster than the decay of the orbital energy, at least if the friction is dominated by cluster stars rather than unbound stars. The binary eccentricity will grow until the resonant friction is quenched by relativistic precession, at which point gravitational radiation may erode the energy of the binary faster than non-resonant dynamical friction. The details of this evolution are relevant to the merger rate of black holes, the gravitational-wave background, the prevalence of binary black holes in AGNs, and the viability of massive black holes as dark matter candidates (see Quinlan 1996 for references).

Resonant friction can also erode the inclination of a massive object in a rotating stellar system. This process may be relevant to a star cluster in which there is a massive accretion disk (Ostriker 1983; Syer et al. 1991); resonant friction could accelerate the evolution of massive stars into low-inclination orbits embedded in the accretion disk.

The analytical treatment of resonant relaxation that we have offered in § 1 is only approximate. Accurate expressions for the resonant and non-resonant relaxation rates in a given star cluster could be derived by expanding the potential from a stellar orbit in action-angle variables. So far this procedure has only been carried out for the dynamical friction component (Weinberg 1986). The relative simplicity of the diffusion coefficients that describe non-resonant relaxation (e.g., Binney & Tremaine 1987) is illusory in near-Keplerian and other near-resonant potentials—except to describe energy relaxation—since resonant relaxation is stronger, and depends more sensitively on the structure of the stellar system. For order-of-magnitude estimates we have used the formulae in § 1, with the dimensionless coefficients given in Table 4.

The estimates of tidal disruption rates in § 3.1 suffer from the absence of a consistent treatment of relativistic precession, which detunes the Kepler resonance near the loss cone in galactic nuclei. However, resonant relaxation is unlikely to increase substantially the tidal disruption rate, which is mostly determined by the location of the critical radius  $r_{\text{crit}}$ , set by the angular momentum changes in a single orbital period. For similar reasons,

resonant relaxation will not greatly affect the disruption rate resulting when the wandering (“Brownian motion”) of the black hole from the center of the nucleus (Quinlan 1995) is taken into account. Thus tidal disruption appears to remain incapable of powering typical AGNs; however, since the relativistic detuning is largely ineffective at hole masses  $\lesssim 10^7 M_\odot$  (eq. 48), resonant effects may offer modest improvements in the feasibility of disruption-dominated mass loss in Seyferts and other nuclei containing low-level AGN activity, for which the energy requirements are less severe. Similarly, resonant relaxation may modestly enhance the rate of flares from tidally disrupted stars in nearby galaxies with central black holes (Rees 1988).

The effectiveness of relativistic precession in disabling resonant relaxation illustrates that general relativity can have dramatic physical consequences even where the motion is predominantly Newtonian; in particular, the shape of the density cusp inside  $r_{\text{crit}}$  can be strongly dependent on relativistic precession. Thus resonant relaxation might one day be used to show that the massive dark objects observed in galactic nuclei are indeed black holes (or at least behave as such on a scale of  $\sim 10^2$  Schwarzschild radii)—a conclusion which today must be reached by indirect (albeit compelling) arguments.

The discussion in §3.1 also illustrates that the Fokker-Planck equation used to describe non-resonant relaxation (e.g. Binney and Tremaine 1987) is not always adequate to describe resonant relaxation. The Fokker-Planck equation assumes that the fluctuating forces at different times and locations are uncorrelated, i.e., that the correlation function of §1.1 has the form  $C_{ij}(\mathbf{r}_1, \mathbf{r}_2, \tau) = K_{ij}(\mathbf{r}_1)\delta(\mathbf{r}_2 - \mathbf{r}_1)\delta(\tau)$ . This is a reasonable approximation for non-resonant relaxation, which is dominated by close encounters (cf. §1.1). In contrast, the resonant forces are correlated over large spatial scales and over times  $\sim t_{\text{prec}}$ . The inadequacy of the Fokker-Planck approximation (or the master equation, or the approximation that relaxation is a Markov process), is particularly acute in the diffusion limit (eq. 43), when the size of the loss cone in angular-momentum space  $L_{\text{min}}$  is much greater than the change in angular momentum per orbit  $\Delta L_{\text{orb}}$  but much less than the change in angular momentum per precession time.

There is an appealing analogy between relaxation of stars in angular-momentum space and models of stellar structure. Non-resonant relaxation is a random walk in  $L$ -space, as for the motion of ions in the radiative zone of a star. Resonant relaxation implies a large-scale drift in  $L$  superimposed upon a small-scale random walk, analogous to ionic motion in a convective stellar envelope. The quenching of resonant relaxation by relativistic precession can produce a random-walk dominated “core” in  $L$ -space surrounded by a drift-dominated envelope—conceptually similar to the radiative core/convective envelope structure found in solar-type stars. There are fundamental differences:  $L$ -space has no analog to gravity, but

there *is* a net flux of stars towards small  $L$  due to removal of stars by tidal disruption.

The structure of a relaxed star cluster surrounding a black hole has been examined by several authors (Peebles 1972; Bahcall & Wolf 1976, 1977; Lightman & Shapiro 1977; Cohn & Kulsrud 1978). These analyses do not take resonant relaxation into account and therefore some of their conclusions may be suspect: we expect that including resonant relaxation will not strongly affect the structure of the star cluster outside the critical radius  $r_{\text{crit}}$  (§ 3.1) or the total flux of stars into the loss cone, but may substantially reduce the density of stars inside  $r_{\text{crit}}$ . This classic problem should be re-investigated.

Resonant relaxation implies that there may be regions near the centers of elliptical galaxies (typically  $\lesssim 1$  pc in radial extent; cf. Table 5) that are relaxed in angular momentum but not energy. If non-rotating, such regions will have isotropic distribution functions; if rotating, the mean rotation speed will depend on the stellar mass. Unfortunately, these regions are not accessible at Hubble Space Telescope resolutions in most nearby galaxies. A more fundamental problem regarding the possible observational detection of resonant relaxation is that the isotropy it produces will be undetectable unless the initial distribution function is significantly anisotropic; there is currently no evidence for this in observed nuclear star clusters.

We thank Jihad Touma for supplying the program to compute the average torque between two Keplerian orbits. This research was supported by NSERC, and by a Jeffrey L. Bishop Fellowship to K. R.

## REFERENCES

- Bahcall, J. N., & Wolf, R. A. 1976, *ApJ*, 209, 214  
———. 1977, *ApJ*, 216, 883  
Bardeen, J. M. 1970, *Nature*, 226, 64  
Begelman, M. C., Blandford, R. D., & Rees, M. J. 1980, *Nature*, 287, 307  
Binney, J., & Tremaine, S. 1987 *Galactic Dynamics* (Princeton: Princeton University Press)  
Chandrasekhar, S. 1942 *Principles of Stellar Dynamics* (Chicago: University of Chicago Press)  
Chandrasekhar, S. 1943, *ApJ*, 97, 255



- Cohen, L. 1973, in *Dynamics of Stellar Systems*, ed. A. Hayli (Dordrecht: Reidel), 33
- Cohn, H., & Kulsrud, R. M. 1978, *ApJ*, 226, 1087
- Darwin, C. 1961, *Proc. Roy. Soc. Lond. A*, 263, 39
- David, L. P., Durisen, R. H., & Cohn, H. N. 1987a, *ApJ*, 313, 556
- . 1987b, *ApJ*, 316, 505
- Duncan, M. J., & Shapiro, S. L. 1983, *ApJ*, 268, 565
- Eckart, A., Genzel, R., Hofmann, R., et al. 1993, *ApJ*, 407, L77
- Faber, S. M., Kormendy, J., Byun, Y.-I., et al. 1996, in preparation
- Frank, J. 1978, *MNRAS*, 184, 87
- Frank, J., & Rees, M. J. 1976, *MNRAS*, 176, 633
- Gebhardt, K., Richstone, D. O., Ajhar, E. A., et al. 1996, *AJ*, submitted
- Hénon, M. 1959, *Ann. d’Astr.*, 22, 126
- Hernquist, L., & Weinberg, M. 1989, *MNRAS*, 238, 407
- Hills, J. G. 1975, *Nature*, 254, 295
- Jeans, J. H. 1913, *MNRAS*, 74, 109
- . 1916, *MNRAS*, 76, 552
- Kent, S. M. 1992, *ApJ*, 387, 181
- Kormendy, J., & McClure, R. D. 1993, *AJ*, 105, 1793
- Kormendy, J., & Richstone, D. 1995, *ARA&A*, 33, 581
- Lightman, A. P., & Shapiro, S. L. 1977, *ApJ*, 211, 244
- Lynden-Bell, D., & Kalnajs, A. J. 1972, *MNRAS* 157, 1
- McMillan, S.L.W., Lightman, A. P., & Cohn, H. N. 1981, *ApJ*, 251, 436
- Murphy, B. W., Cohn, H. N., & Durisen, R. H. 1991, *ApJ*, 370, 60
- Norman, C., & Scoville, N. 1988, *ApJ*, 332, 124

- Ostriker, J. P. 1973, unpublished lectures at Princeton University
- Ostriker, J. P. 1983, *ApJ*, 273, 99
- Peebles, P. J. E. 1972, *Gen. Rel. Grav.* 3, 63.
- Polnarev, A. G., & Rees, M. J. 1994, *A&A*, 283, 301
- Quinlan, G. D. 1995, unpublished notes from the Aspen workshop “Physics of Dense Stellar Systems”
- Quinlan, G. D. 1996, submitted to *NewA*
- Quinlan, G. D., & Shapiro, S. L. 1990, *ApJ*, 356, 483
- Rees, M. J. 1988, *Nature*, 333, 523
- Spitzer, L., & Stone, M. E. 1967, *ApJ*, 147, 519
- Syer, D., Clarke, C. J., & Rees, M. J. 1991, *MNRAS*, 250, 505
- Thorne, K. S. 1974, *ApJ*, 191, 507
- Touma, J., & Tremaine, S. 1996, in preparation
- Tremaine, S., & Weinberg, M. D. 1984, *MNRAS*, 209, 729
- Weinberg, M. D. 1986, *ApJ*, 300, 93
- Yoshida, H. 1990, *Phys. Lett. A*, 150, 262